Numerical simulations of optical parametric amplification cross-correlation frequency-resolved optical gating

Xuan Liu, Aparna Prasad Shreenath, Mark Kimmel, and Rick Trebino

School of Physics, Georgia Institute of Technology, Atlanta, Georgia 30332-0430

Arlee V. Smith

Sandia National Laboratories, Albuquerque, New Mexico 87185

Stephan Link

Center for Nano- and Molecular Science and Technology, University of Texas at Austin, Austin, Texas 78712

Received April 12, 2005; revised August 24, 2005; accepted August 30, 2005

We perform numerical simulations of cross-correlation frequency-resolved optical gating with the nonlinearities, optical parametric amplification, and difference-frequency generation for measuring broadband pulses. We show that use of a noncollinear beam geometry that matches the group velocities of the pump, signal, and idler pulses permits use of relatively thick crystals for high gain without significant distortion in the measured trace, yielding bandwidths of ~100 nm. © 2006 Optical Society of America

OCIS codes: 190.4410, 190.7110, 300.6420, 300.6530.

1. INTRODUCTION

Since the introduction of frequency-resolved optical gating (FROG),[1–3] there has been tremendous progress in the development of techniques to measure the intensity and phase versus time of ultrashort pulses. Although FROG and its many variations, including cross-correlation FROG (XFROG),[4] allow the measurement of a wide range of pulses, these techniques do not yet have the sensitivity to measure extremely weak ultrashort light pulses—whose measurement would be useful to understand many important fundamental light emission processes.[5] Although linear techniques such as spectral interferometry (SI) are much more sensitive, with demonstrated measurements of zeptojoule pulses on a multishot basis,[6] the drawback is that they require nearly perfect spatial and temporal coherence of the unknown pulse in addition to the necessity of a well-characterized reference pulse whose spectrum spans that of the unknown pulse. As a result, we recently introduced a noninterferometric technique that avoids such restrictive coherence requirements: XFROG, using the nonlinearity of optical parametric amplification (OPA) which improves the sensitivity enough to measure pulses as weak as a 50 aJ.[7] We showed that the phase of the pulse to be measured is not modified by the gating process, making its retrieval quite straightforward by use of a slightly modified XFROG algorithm. This new technique (OPA XFROG) can be considered more sensitive than even SI because the total number of photons involved in our lower-repetition-rate measurement was lower by a factor of 100,000 than the previously demonstrated record of 42 zeptojoules measured with SI.

In our previous work on OPA XFROG, an issue that remained unanswered was the trade-off between accuracy and efficiency. Specifically, the accuracy requirement requires that we minimize the group-delay mismatch (GDM) in the crystal between the two (or three) pulses involved to minimize geometrical smearing of the temporal features of the pulse to be measured, which otherwise would yield inaccurate results. The efficiency requirement, on the other hand, involves maximizing the gain in the nonlinear process. Short crystals yield high accuracy but low efficiency: They typically achieve minimal GDM (GDM is proportional to L, where L is the crystal length) and hence yield high OPA XFROG accuracy, but they also yield minimal gain. Long crystals, on the other hand, yield high efficiency but low accuracy: They yield high gain, but they also tend to have large GDM and thus tend to potentially yield some distortion in the measurement.

A similar problem has cropped up previously, and that is in OPA devices used to efficiently transform pulses from one wavelength to another. In that field, this problem was solved by use of noncollinear OPA (NOPA)[8–10] beam geometries with a few degrees between the two beams, which yield considerably larger phase-matching bandwidths or, equivalently, much smaller GDM. Clearly, the NOPA concept will also provide a useful approach for OPA XFROG measurements. The OPA XFROG problem, however, is somewhat different from that of NOPAs for efficient wavelength conversion. While efficiency is the predominant goal in NOPAs, whose only requirement on the generated pulse is that it have approximately the same duration as the input pump pulse, our requirement is much more stringent: We require that the intensity and phase

of this pulse be such that it can be accurately modeled and, in particular, we would prefer it to have the ideal form:

$$E_{\mathrm{sig}}^{\mathrm{OPA}}(t,\tau) = E(t)E_{\mathrm{gate}}^{\mathrm{OPA}}(t-\tau), \tag{1}$$

where $E(t)$ is the unknown input pulse; the second factor is the gate function, given by

$$E_{\mathrm{gate}}^{\mathrm{OPA}}(t) = \cosh(g|E_{\mathrm{ref}}(t)|z), \tag{2}$$

where $E_{\mathrm{ref}}(t)$ is the reference (pump) pulse and g is the parametric gain coefficient.[7]

On the other hand, OPA XFROG has the simplification that it does not involve, or even desire, efficient conversion of the pump pulse energy to the signal. In other words, OPA XFROG, unlike wavelength conversion NOPAs, does not operate in the pump depletion regime. This is a major simplification.

The goal of this paper is therefore to numerically model the OPA XFROG process for typical experimental conditions, synthesizing XFROG traces that are then fed to the XFROG algorithm to check the accuracy of the extracted pulse amplitude and phase profiles. We show that perfect group-velocity matching of the three pulses yields excellent accuracy with large bandwidths in such measurements even in the presence of high gain. We also analyze difference-frequency generation (DFG) XFROG and show that our simple model works just as well for DFG XFROG as it does for OPA XFROG. Our theoretical simulations show that it is possible to retrieve the unknown pulse by making either an OPA measurement or a DFG measurement and applying the suitable XFROG algorithm. Indeed, while it should be possible to develop a complete and precise FROG algorithm for these techniques in the general case, we show that, when group-velocity matching occurs, the simple, ideal expressions for the trace [Eqs. (1) and (2)] work well. Finally, We report an experimental demonstration using a ~100 nm wide pulse spectrally filtered from a continuum.

2. OPA AND DFG XFROG

The OPA or DFG XFROG scans a short, well-characterized gate pulse across the unknown signal pulse to parametrically amplify a short portion of it. The output pulses at signal–idler frequencies are spectrally resolved, yielding the typical XFROG traces of spectrum versus time. The expression for a XFROG trace is[3]

$$I_{\mathrm{XFROG}}(\omega,\tau) = \left| \int_{-\infty}^{\infty} E(t)E_{\mathrm{gate}}(t-\tau)\exp(-i\omega t)\mathrm{d}t \right|^2. \tag{3}$$

We call the process OPA XFROG if the signal trace is analyzed to reconstruct the unknown signal and DFG XFROG if the idler frequency trace is used. The standard FROG algorithm is easily modified to deal with XFROG (both are available commercially) to extract the pulse intensity and phase.

In this section we will discuss a simplified, ideal-case theory of OPA and DFG and a simplified algorithm for OPA and DFG XFROG. We will revisit the theory more rigorously in Section 3. Assuming negligible pump depletion, perfect group-velocity matching, and phase matching, the coupled-wave equations for the generation of both the signal and the idler are[11]

$$\frac{\partial E_{\mathrm{OPA}}}{\partial z} = i\kappa E_{\mathrm{ref}}E_{\mathrm{DFG}}^{*}, \tag{4}$$

$$\frac{\partial E_{\mathrm{DFG}}}{\partial z} = i\kappa' E_{\mathrm{ref}}E_{\mathrm{OPA}}^{*}, \tag{5}$$

where $\kappa = 2\pi d_{\mathrm{eff}}/(n_{\mathrm{OPA}}\lambda_{\mathrm{OPA}})$ and $\kappa' = 2\pi d_{\mathrm{eff}}/(n_{\mathrm{DFG}}\lambda_{\mathrm{DFG}})$.

The pulse to be measured experiences exponential gain during the OPA process and its phase is well preserved, shown by Eqs. (1) and (2).

For DFG XFROG, the electric field is given by

$$E_{\mathrm{sig}}^{\mathrm{DFG}}(t,\tau) = E(t)E_{\mathrm{gate}}^{\mathrm{DFG}^{*}}(t-\tau), \tag{6}$$

with a gate function of the form

$$E_{\mathrm{gate}}^{\mathrm{DFG}}(t) = \exp[i\phi_{\mathrm{ref}}(t)]\sinh[g|E_{\mathrm{ref}}(t)|z], \tag{7}$$

where $\phi_{\mathrm{ref}}(t)$ is the phase of the reference pulse. Unlike OPA XFROG, no background is present at large delays in DFG XFROG.

The temporal resolution of the OPA–DFG XFROG trace is provided by the short gating pump pulse, so high time resolution requires that the temporal walk-off among the signal pulse, the idler pulse, and the pump pulse be small. This can be accomplished by using short crystals or by matching the group velocities of the three pulses. Group-velocity matching is preferred because it permits use of long crystals, which increases the parametric gain and thus the sensitivity of the technique. We will show that in some circumstances it is possible to match the effective group velocities of all three pulses by adjusting the crossing angles of the beams while keeping the pulse envelopes parallel. If the group velocities are matched, the fidelity of the method is limited by the group-delay dispersion of the pulses. In Section 3 we numerically simulate the OPA XFROG and DFG XFROG processes to study the influence of group-velocity mismatch and group-delay dispersion on the accuracy of these methods. We note that the strict angle requirements for group-velocity matching make it difficult to adapt OPA XFROG to angle-dispersed single-shot geometries.[12]

3. THEORY

In this section we will investigate the theory of OPA and DFG more rigorously. We derive a set of equations to describe the parametric mixing process of three temporally structured waves that propagate at different angles.

We define our fields in terms of a carrier frequency ω_j ($j=s$, i, and p refers to the signal, idler, and pump, respectively) by

$$E_j(t,z) = \frac{1}{2}\{E_j(t,z)\exp[-i(\omega_j t - k_j z)] + E^{*}{}_j(t,z)\exp[i(\omega_j t - k_j z)]\}. \tag{8}$$

Under the slowly varying amplitude approximation, with pulse envelopes normal to z, the three-wave parametric mixing equations for the collinear case are[13]

$$\left(\frac{\partial}{\partial z}+\frac{1}{V_s}\frac{\partial}{\partial t}+i\frac{1}{2}\frac{\partial^2 k_s}{\partial\omega^2}\frac{\partial^2}{\partial t^2}\right)E(t,z)=\frac{i\omega_s}{n_s c}d_{\text{eff}}E_p E_i^* \exp(i\Delta kz), \tag{9}$$

$$\left(\frac{\partial}{\partial z}+\frac{1}{V_i}\frac{\partial}{\partial t}+i\frac{1}{2}\frac{\partial^2 k_i}{\partial\omega^2}\frac{\partial^2}{\partial t^2}\right)E(t,z)=\frac{i\omega_i}{n_i c}d_{\text{eff}}E_p E_s^* \exp(i\Delta kz), \tag{10}$$

$$\left(\frac{\partial}{\partial z}+\frac{1}{V_p}\frac{\partial}{\partial t}+i\frac{1}{2}\frac{\partial^2 k_p}{\partial\omega^2}\frac{\partial^2}{\partial t^2}\right)E(t,z)=\frac{i\omega_p}{n_p c}d_{\text{eff}}E_s E_i \exp(-i\Delta kz), \tag{11}$$

where d_{eff} is the effective nonlinearity and n_j is the effective refractive index. $\Delta k=k_p-k_s-k_i$ is the phase mismatch and V_j is the group velocity.

For noncollinear parametric mixing, diagrammed in Fig. 1, the three beams are tilted. The group-velocity and the group-delay dispersion factors will be modified[14] by this tilt. We define the modified group-velocity and group-delay dispersion as the apparent group-velocity and apparent group-delay dispersion indicated by $\hat{V}_g$ and $\hat{D}$:

$$\hat{V}_g=V_g\frac{\cos(\alpha+\phi+\rho)}{\cos\phi\cos\rho}, \tag{12}$$

$$\hat{D}=-\frac{1}{2}\frac{\mathrm{d}^2 k_z}{\mathrm{d}\omega^2}=\frac{1}{2{V_g}^2}\frac{\cos\phi\cos\rho}{\cos(\alpha+\phi+\rho)}\text{GVD}+\frac{1}{{V_g}^2}\frac{\cos\phi\cos^3\rho\sin^2(\alpha+\phi)}{\cos^3(\alpha+\phi+\rho)}A. \tag{13}$$

Here V_g is the group velocity along the direction of the k vector of the pulse's carrier wave and GVD is the ordinary group-velocity dispersion. ϕ is the slant angle of the pulse front relative to the normal to the z axis. α is the tilt angle of the propagation vector, assumed to lie in the same plane as the birefringent walk-off ρ. The above apparent group-delay dispersion is slightly different from the equation in Ref. 14 because we are using a more accurate coefficient for the diffraction. Instead of using $1/(2k)$, we now use A[15]:

$$A=\frac{1}{2k}-\frac{1}{2k^2}\frac{\partial^2 k}{\partial\alpha^2}. \tag{14}$$

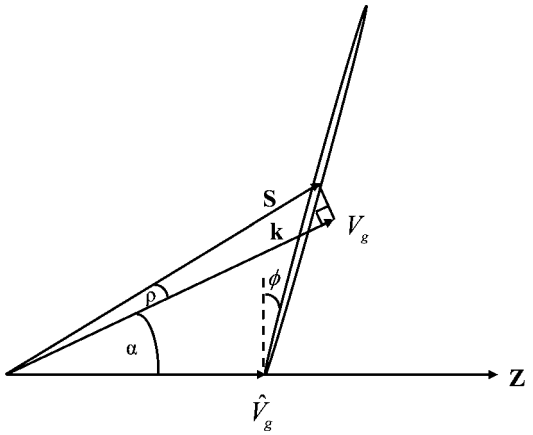

Fig. 1. Apparent group velocity ($\hat{V}_g$) of a slanted pulse. The propagation vector is tilted by α relative to the z axis, and V_g is the group velocity of an unslanted pulse. The birefringent walk-off angle is ρ, and ϕ is the slant angle of the pulse front relative to the normal to the z axis.

Substituting the above expressions into Eqs. (9)–(11) we then have the wave equations for the noncollinear parametric mixing:

$$\frac{\partial E_j}{\partial z}+\frac{1}{\hat{V}_{gj}}\frac{\partial E_j}{\partial t}-i\hat{D}\frac{\partial^2 E_j}{\partial t^2}=\tilde{P}_j, \tag{15}$$

where

$$\tilde{P}_s=\frac{i\omega_s}{\tilde{n}_s c}d_{\text{eff}}E_p E_i^* \exp(i\Delta kz), \tag{16}$$

$$\tilde{P}_i=\frac{i\omega_i}{\tilde{n}_i c}d_{\text{eff}}E_p E_s^* \exp(i\Delta kz), \tag{17}$$

$$\tilde{P}_p=\frac{i\omega_p}{\tilde{n}_p c}d_{\text{eff}}E_s E_i \exp(-i\Delta kz). \tag{18}$$

Here $\tilde{n}_j$ is the effective refractive index, defined by

$$\tilde{n}_j=\begin{cases} n_j\cos\rho_j\cos(\alpha_j+\rho_j) & x \text{ polarized} \\ n_j\cos\alpha_j & y \text{ polarized}\end{cases}. \tag{19}$$

This modification of the refractive index emerges for beams tilted by α with respect to the z axis.[16]

It is reasonable to expect that the requirements for the highest accuracy are that the three pulses remain perfectly overlapped in time as they travel through the crystal. Smith[14] has demonstrated that it is possible to achieve exact group-velocity matching of all three pulses by use of a combination of pulse-front tilt (prisms and gratings can induce the appropriate pulse-front tilt[17]) and noncollinear phase matching. Possible crystals and angles can be calculated using the nonlinear optical software SNLO[18] GVM function. For example, for 390–600 nm, 1114.3 nm crystals β-barium borate (BBO), KABO, KBBF, and lithiumtriborate can all provide near-perfect group-velocity matching. Among these crystals BBO has the highest nonlinear coefficient and is our choice. For a type I parametric process, we find the crossing angle between the pump and the signal beams that permits the group-velocity-matched mixing to be 7.15° using SNLO.[18] No pulse-front tilt is needed for the pump pulse. This idealized case is shown in Fig. 2. (For convenience, we align $\hat{k}_p$ along $\hat{z}$.) The temporal structure within the signal pulse is assumed to be parallel to the pump envelope.

We integrate the mixing equations, Eqs. (15)–(18), for each of a range of values of delay between the signal pulse and the pump pulse to synthesize an XFROG trace. The 600 nm signal pulse is 850 fs long, and the 390 nm pump pulse is 120 fs long. The input energies of the signal and pump pulses are 5 fJ and 8 μJ/pulse, respectively.

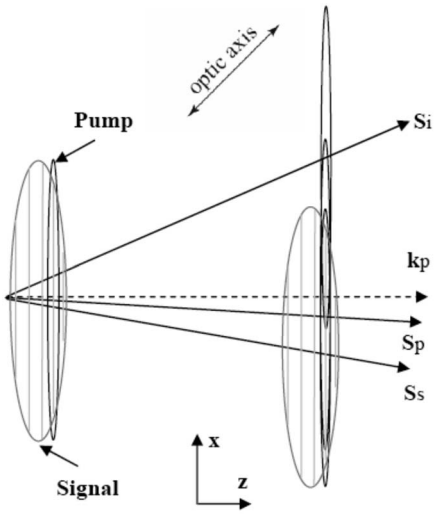

Fig. 2. Requirements for the highest accuracy. The signal crosses the pump at an angle. The gray lines inside the signal represent the temporal structure.

We assume Gaussian temporal input intensity profiles for our pulses. The fluences are 1.103×10^{-11} and 7.845×10^{-3} J/cm^2 for the signal and pump, respectively. We also assume that the phase-matching conditions are satisfied exactly for the central frequency, or carrier waves of the pulses. In all the calculations we use $d_{\text{eff}}=1.8$ pm/V. The number of time steps is 512 and the number of z steps is 30. We use a split-step, fast-Fourier-transform method to integrate the equations, ignoring any transverse structure of the waves. We investigate the effect of different crystal thicknesses, as well as different beam crossing angles on pulse retrievals using the OPA XFROG algorithm. Our grid size for the FROG trace is 512 by 512 in the spectral and delay dimensions. Unless specified otherwise, we use the above parameters in our calculations. We use a linearly chirped broadband input pulse and a flat-phase pump pulse.

We begin with the idealized case in which all three pulses travel at exactly the same group velocity and there is no group-velocity dispersion. The resulting OPA XFROG trace is shown in Fig. 3(a). The corresponding retrieved trace is shown in Fig. 3(b) using the ideal-case OPA XFROG algorithm, which yields a very low FROG error of 4.339×10^{-5}. Figures 3(c) and 3(d) show the retrieved temporal and spectral pulse intensities and phases compared with the actual pulse temporal and spectral intensities and phases. The agreement is excellent. Both the retrieved and the actual pulses have the same FWHM of 72 nm.

Figure 4 shows a typical configuration of our experiment. At the input to the crystal there is a short, strong pump pulse and a weak, longer input pulse. At the output of the crystal, coincident with the pump pulse, there is a strong idler pulse and a strong segment of the signal pulse, plus the weak, unamplified input pulse. We assume that the beams are large and uniform in irradiance in the transverse dimension, so diffraction and transverse irradiance profiles can be ignored in our simulations. We show that we can make the OPA XFROG measurements with little GVM-induced distortion if we cross the pump and the signal at the predicted velocity-matching angle of 7.15°. We simulated the case when using a 2 mm (the effective interacting length could be much less when tightly focused input beams are used) BBO crystal (see Fig. 5), including the group-delay dispersion terms. The FWHM of the retrieved signal pulse is estimated to be 63 nm, which is 9 nm narrower than the ideal 72 nm input seed pulse. The peak parametric gain is found in the simulation to be 1.2×10^7 and no pump depletion is observed.

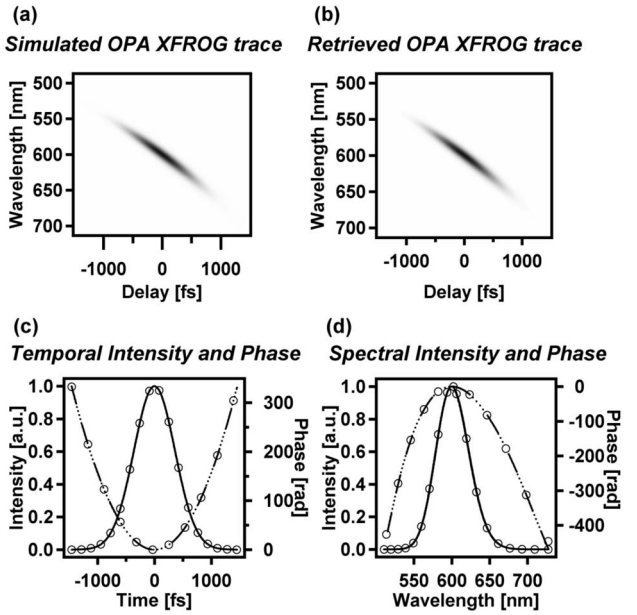

Fig. 3. (a) Ideal OPA XFROG trace of a pulse and (b) its retrieval with a 2 mm thick BBO crystal. The FROG error was 4.339×10^{-5}. The solid curves with circular markers in (c) and (d) show the retrieved temporal and spectral intensities of the pulse. The dotted curves with circular markers refer to the retrieved signal temporal and spectral phases. The solid curves without any markers refer to the intensities of the actual pulse. The dashed curves without any markers are the corresponding phases of the actual pulse.

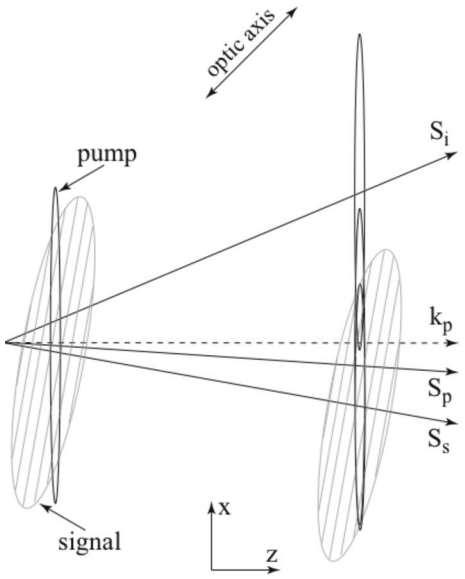

Fig. 4. Typical configuration of our experiments. The gray lines inside the signal represent the temporal structure.

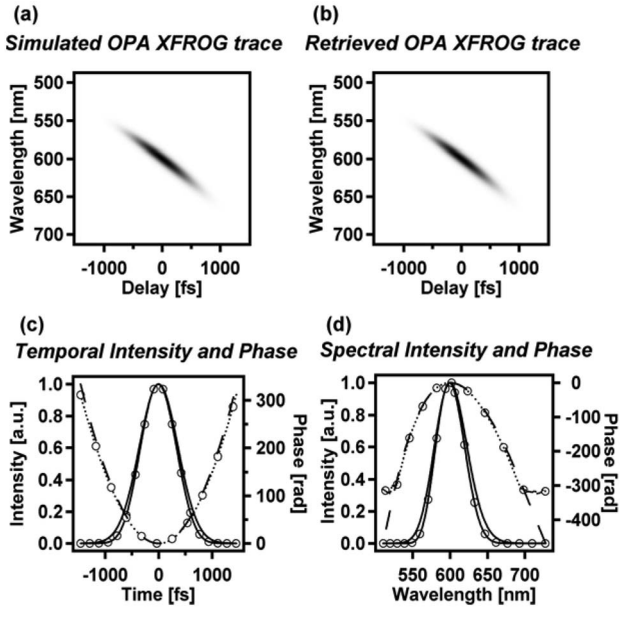

Fig. 5. OPA XFROG trace and its retrieval with a 2 mm thick BBO crystal (conventions are the same as in Fig. 3). The crossing angle between the pump and the input pulse is 7.15°. The FROG error was 4.102×10^{-4}.

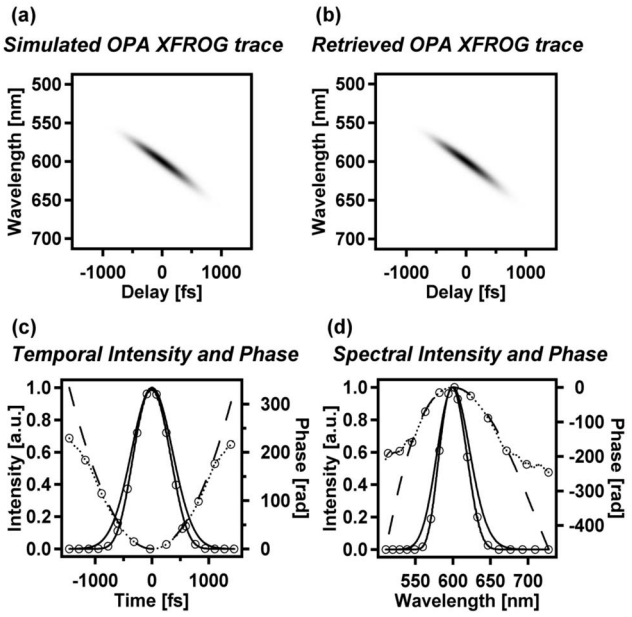

Fig. 6. OPA XFROG trace of the signal and its retrieval with a 3 mm BBO crystal (conventions are the same as in Fig. 3). The input energy of the pump is 2 μJ. The FROG error was 4.254×10^{-4}.

The temporal and spectral phases retrieve quite well. Overall, the retrieved pulse shows a low FROG error of 4.102×10^{-4}.

When the crossing angle is 7.15°, the group velocities of the three pulses are nearly equal along the propagation axis (z axis), and the bandwidth narrowing caused by GVM is negligible. The observed narrowing is caused primarily by the apparent GVD of the three pulses of −42.839, 78.854, and −95.553 fm^2/mm for the signal, idler, and pump, respectively.

This GVD narrowing becomes more significant in thicker crystals as illustrated in Fig. 6 where we use a 3 mm long crystal and, to avoid depletion, a reduced pump pulse energy of 2 μJ and fluence of 1.961×10^{-3} J/cm^2. The peak parametric gain is reduced to approximately 1.5×10^5. The retrieved signal pulse in the 3 mm crystal has a FWHM of 57 nm compared with 63 nm for the 2 mm crystal. Figure 7 shows the case of a 1 mm thick BBO crystal with a 30 μJ pump with a fluence of 2.942×10^{-2} J/cm^2. The peak parametric gain is

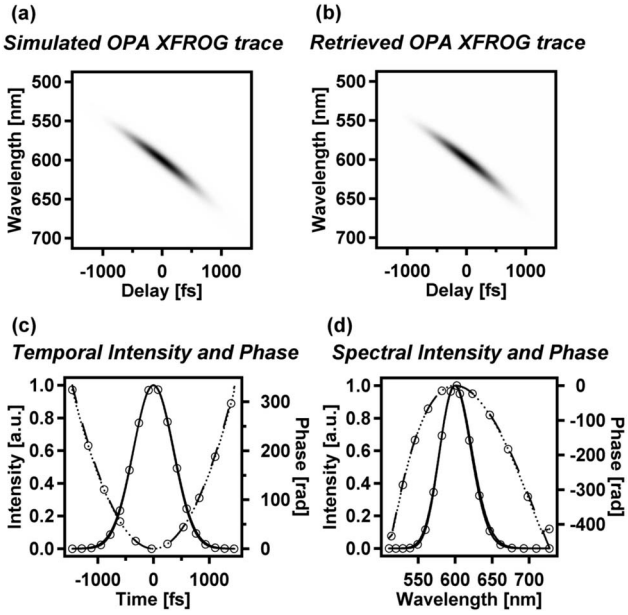

Fig. 7. OPA XFROG trace and its retrieval with a 1 mm thick BBO crystal (conventions are the same as in Fig. 3). The input energy of the pump was 30 μJ. The FROG error was 2.547×10^{-4}.

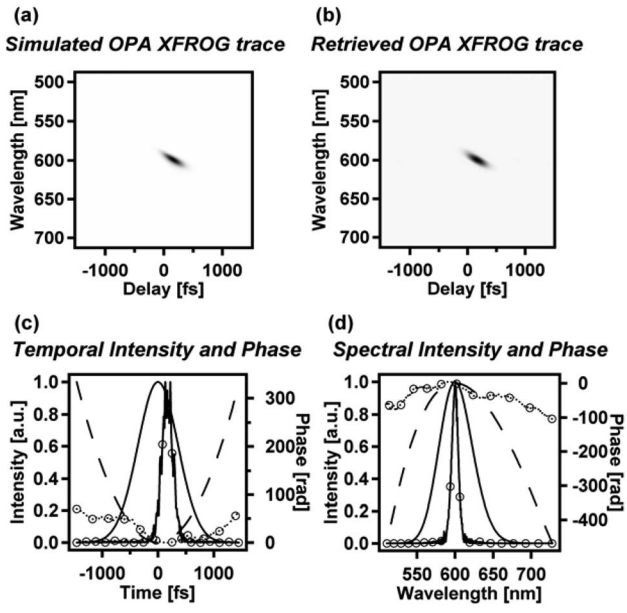

Fig. 8. OPA XFROG trace and its retrieved pulse with collinear beams ($\alpha_s=0°$; conventions are the same as in Fig. 3). The FROG error was 5.250×10^{-3}. The retrieved spectral FWHM was 14 nm.

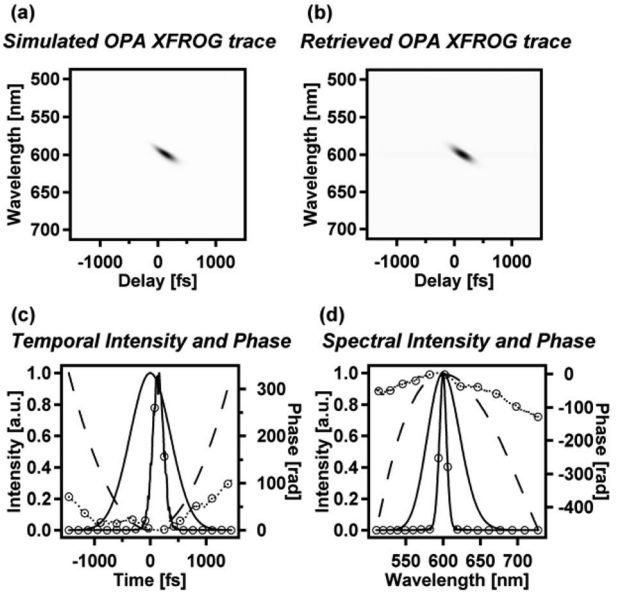

Fig. 9. OPA XFROG trace and its retrieved pulse with crossing angle $\alpha_s=3°$ (conventions are the same as in Fig. 3). The FROG error was 5.844×10^{-3}. The retrieved spectral FWHM was 16 nm.

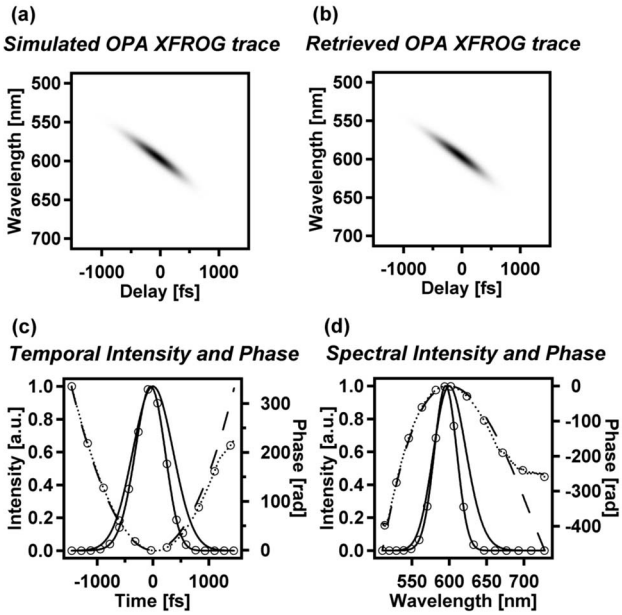

Fig. 10. OPA XFROG trace and its retrieved pulse with a crossing angle $\alpha_s=6.52°$ (conventions are the same as in Fig. 3). The FROG error was 1.500×10^{-3}. The retrieved spectral FWHM was 50 nm.

$\sim7\times10^6$. With this thinner crystal we observe little spectral narrowing. Our OPA XFROG algorithm retrieves the input signal spectral width of 69 nm with a very low error of 2.547×10^{-4}. For each of the crystal lengths, the spectral phase is quite accurately retrieved.

We next tested the importance of group-velocity matching. We expect that a slight temporal walk-off of any of the pulses can distort the amplified signal pulse and the retrieved pulse. Choosing the right crossing angle between the pump pulse and the input pulse is critical. In Figs. 8–11 we show XFROG traces of the signal and their retrievals with the crossing angles of 0°, 3°, 6.52°, and 10°, respectively, in a 2 mm long crystal.

For the collinear geometry, $\alpha_s=0°$, we obtain a pulse with only 14 nm of bandwidth after parametric amplification (see Fig. 8). When the signal is tilted away from the pump by a small angle of 3°, the signal bandwidth becomes 16 nm (see Fig. 9). When the signal and the pump are crossed at 6.52°, the retrieved pulse has a bandwidth of 50 nm (see Fig. 10). If we deviate from the ideal crossing angle, 7.15° in the other direction and use 10° instead, the bandwidth also decreases to 14 nm (see Fig. 11).

If perfect group-velocity matching is achieved, the limit on crystal length is set by group-delay dispersion that also distorts the amplified pulses if the crystal is longer than the dispersion length of $L_{\mathrm{gdd}}=\tau^2/4\hat{D}$ where $\hat{D}$ is the apparent group-delay dispersion, and τ is the shortest time we want to resolve, normally one half or one fourth of the pump duration.

We now show simulations of DFG XFROG, which also allows the measurement of pulses with gain. We consider the same configurations as for OPA XFROG in a 2 mm type I BBO crystal with a 7.15° crossing angle between the signal and pump, but use the idler pulse to retrieve the input signal pulse. We plot the resulting DFG XFROG traces and corresponding retrieved pulses in Fig. 12. The retrieved signal spectral width is 63 nm, identical to that retrieved from the corresponding OPA XFROG simulation. The FROG error in this case was 5.922×10^{-4} compared with 4.102×10^{-4} for the OPA XFROG retrieval.

4. EXPERIMENT

The schematic for our experimental setup for OPA–DFG XFROG is shown in Fig. 13. Either the signal or the idler pulse can be spectrally resolved to yield an OPA XFROG or DFG XFROG trace. We use a KM Labs Ti: sapphire os-

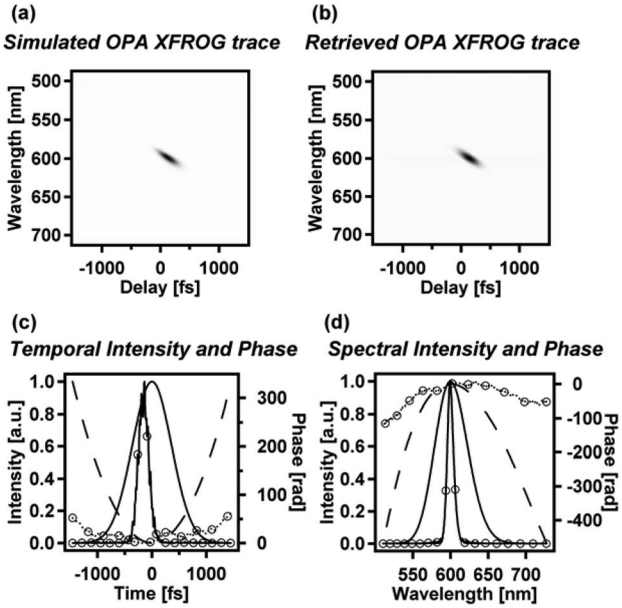

Fig. 11. OPA XFROG trace and its retrieved pulse with a crossing angle $\alpha_s=10°$ (conventions are the same as in Fig. 3). The FROG error was 5.863×10^{-3}. The retrieved spectral FWHM was only 14 nm.

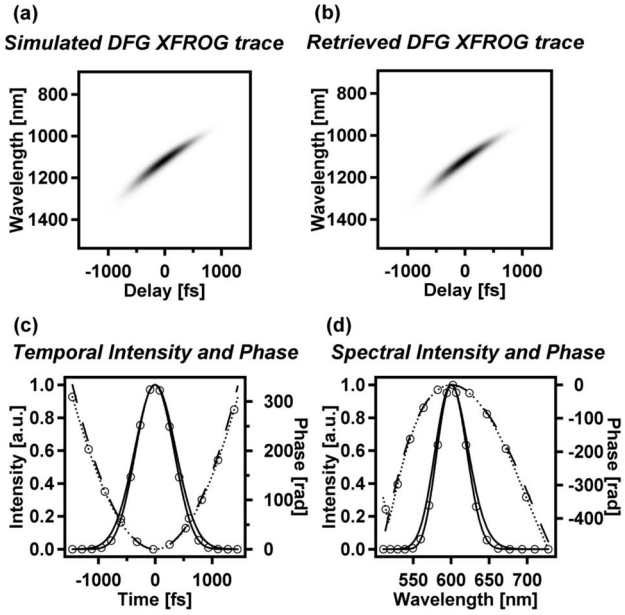

Fig. 12. (a) DFG XFROG trace of a pulse and (b) its retrieval with a 2 nm thick BBO crystal. The FROG error was 5.922×10^{-4}. The solid curves with circular markers in (c) and (d) show the retrieved temporal and spectral intensities of the signal pulse. The dotted curves with circular markers refer to the retrieved signal temporal and spectral phases. The solid curves without any markers refer to the intensities of the actual signal pulse. The dashed curves without any markers are the corresponding phases of the actual signal pulse.

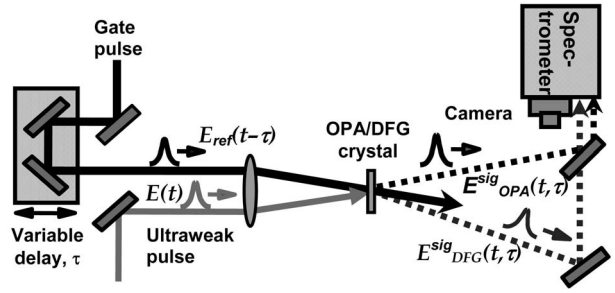

Fig. 13. Schematic of the experimental apparatus for OPA–DFG XFROG. The gate pulse is characterized using a GRENOUILLE (not shown) before it enters the XFROG setup.

cillator, amplified using a kilohertz-repetition-rate regenerative amplifier to create a strong 800 nm pulse. We characterized this pulse using a Swamp Optics GRENOUILLE Model 8–50. The pulse was frequency doubled in a 1 mm thick type I BBO crystal with a deliberately low conversion efficiency of 15%. The fundamental and the second-harmonic pulses were separated using a harmonic separator to form the first component of the OPA XFROG device. In one arm of the XFROG setup, the fundamental pulse was used to generate a white-light continuum (with poor spatial coherence) in a 2 mm thick sapphire plate, which was then spectrally filtered using a combination of BG40 and OG515 filters to yield a slice of the spectrum ~60 nm wide centered on 600 nm. This energy of the filtered pulse was 500 pJ but it was attenuated by a factor of 105 using neutral-density filters to yield an ~5 fJ pulse. This unknown pulse was focused into the 2 mm thick type I BBO crystal using a 100 mm focal-length lens. The spot size at the crystal for the pump and the seed pulses was 265 and 120 μm, respectively. The 8.0 μJ, 400 nm second-harmonic pulse in the other arm of the XFROG device passed through a variable length path to provide the variable gate pulse delay. This pump pulse was focused into the nonlinear crystal separately from the white light using a 75 mm focal-length spherical mirror. The white light and the pump pulse crossed at an internal angle of ~6.5° in the BBO crystal. The thickness of the crystal was short enough that the effects of GVM were small compared to the pulse length, permitting use of the simple gate functions described above. This geometry provided ample phase-matching bandwidth to cover the seed pulse bandwidth. The resulting OPA signal at the CCD array was integrated over a few seconds. The OPA signal emerging from the BBO crystal experienced an average gain (G) of approximately $\cosh(8) \sim 1490$ (see Fig. 14), which, in view of the weak pulses involved, still easily satisfied the condition of negligible pump depletion. This gain was less than predicted by our simulation, but beam alignment, beam quality issues, and beam lateral walk-off probably account for this. The gain bandwidth is not reduced by the limited beam size or walk-off. The observed gain was more than sufficient to record the spectrally dispersed OPA XFROG signal at the camera. The OPA XFROG retrieved pulse had a FROG error of 0.0216. Its duration was approximately 850 fs with a spectral width of 60 nm. The fine structure in the retrieved intensity and spectrum complicated an exact FWHM determination, so we estimated these values from a fitted curve. Although these numbers implied a small amount of distortion due to GVM, in light of our earlier simulations, we chose what we considered a happy medium between high parametric gain and low distortion, where we were still well within the regime where the spectral phase has not been compromised. Geometrical smearing[19] in this measurement was negligible compared to the length of the pulse. The smearing in the longitudinal direction was ~32 fs, whereas the transverse smearing was 20 fs.

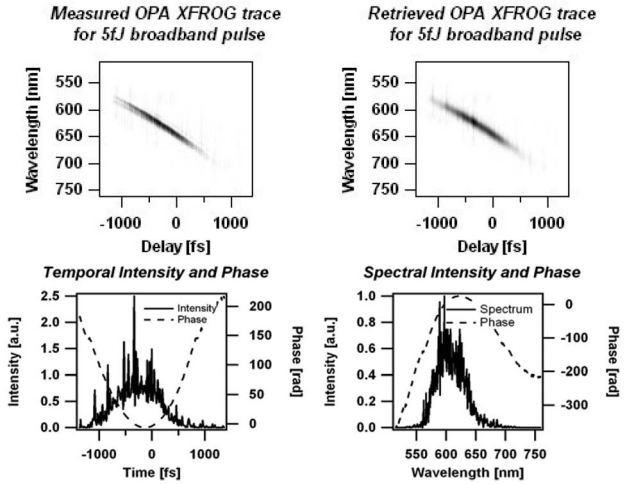

Fig. 14. Measured and retrieved OPA XFROG measurements of a broadband white-light continuum for a pulse of 5 fJ, showing a gain of ~1490.

The fine structure observed in the temporal and spectral intensity plots is characteristic of the continuum pulse, rather than an artifact of our experiment or the retrieval algorithm. We routinely observe such previously highly structured broadband continuum pulses from microstructure fibers.[20] Numerical simulations and single-shot measurements of such a continuum also show that the spectrum of such a pulse is highly structured due to higher-order nonlinear processes involved in the generation of white light.[21,22] In our case, even a single-shot measurement of the white-light spectrum will be unable to measure this highly complex structure, because we have deliberately generated white light from multiple filaments in the white-light source to emulate the spatial incoherence property of fluorescence (to which we anticipate OPA XFROG will be applied) as well as we could. This causes the spectral features to tend to wash out on a single-shot spectral measurement, but FROG measurements are able to see it due to the additional information in the FROG time- and frequency-domain measured traces.

5. CONCLUSIONS

We have validated by numerical modeling the new variation of the FROG technique, called OPA XFROG, which, along with its cousin DFG XFROG, is the most sensitive technique for ultrashort-light-pulse measurement now available. Unlike interferometric methods, it does not carry prohibitively restrictive requirements, such as perfect mode matching, perfect spatial coherence, highly stable absolute phase, and a same-spectrum reference pulse. We have shown that, while care must be taken to avoid GVM effects in such measurements for femtosecond pulses, this problem can be solved by using appropriate broadband crossed-beam geometries that permits use of relatively thick crystals and high parametric gains. This makes OPA and DFG XFROG powerful tools to measure nonlaser ultrashort light pulses. We previously demonstrated that OPA XFROG can measure the intensity and phase versus time for pulses with only a few attojoules per pulse and with pulse widths of the order of 250 fs; now we have shown that much broader bandwidth pulses can also be measured accurately. By increasing the pump power (despite the limits imposed by competing OPG processes), it should be possible to measure ultraweak pulses of the order of a few hundred zeptojoules (i.e., just a few photons per pulse). DFG XFROG has the same sensitivity and should be ideal to measure light pulses in the infrared, although broadband beam geometries remain to be considered for these wavelengths. More importantly, we believe that it should be possible to use OPA XFROG to measure ultraweak, ultrafast fluorescence from biologically important nonfluorescent media.

ACKNOWLEDGMENTS

This material is based on work supported by the National Science Foundation under grant DBI-0116564.

REFERENCES

1. D. J. Kane and R. Trebino, "Characterization of arbitrary femtosecond pulses using frequency resolved optical gating," IEEE J. Quantum Electron. **29**, 571–579 (1993).
2. R. Trebino and D. J. Kane, "Using phase retrieval to measure the intensity and phase of ultrashort pulses: frequency-resolved optical gating," J. Opt. Soc. Am. B **10**, 1101–1111 (1993).
3. R. Trebino, *Frequency-Resolved Optical Gating: the Measurement of Ultrashort Laser Pulses* (Kluwer Academic, 2002).
4. S. Linden, H. Giessen, and J. Kuhl, "XFROG—a new method for amplitude and phase characterization of weak ultrashort pulses," Phys. Status Solidi B **206**, 119–124 (1998).
5. P. Miller, ed., *Ultrafast Phenomena XIII*, (Springer-Verlag, 2003).
6. D. N. Fittinghoff, J. L. Bowie, J. N. Sweetser, R. T. Jennings, M. A. Krumbügel, K. W. DeLong, R. Trebino, and I. A. Walmsley, "Measurement of the intensity and phase of ultraweak, ultrashort laser pulse," Opt. Lett. **21**, 884–886 (1996).
7. J. Y. Zhang, A. P. Shreenath, M. Kimmel, E. Zeek, R. Trebino, and S. Link, "Measurement of the intensity and phase of attojoule femtosecond light pulses using optical-parametric-amplification cross-correlation frequency-resolved optical gating," Opt. Express **11**, 601–609 (2003).
8. G. Cerullo and S. De Silvestri, "Ultrafast optical parametric amplifiers," Rev. Sci. Instrum. **74**, 1–18 (2003).
9. E. Riedle, M. Beutter, S. Lochbrunner, J. Piel, S. Schenkl, S. Sporlein, and W. Zinth, "Generation of 10 to 50 fs pulses tunable through all of the visible and the NIR," Appl. Phys. B **71**, 457–465 (2000).
10. V. Krylov, J. Gallus, U. P. Wild, A. Kalintsev, and A. Rebane, "Femtosecond noncollinear and collinear parametric generation and amplification in BBO crystal," Appl. Phys. B **70**, 163–168 (2000).
11. R. W. Boyd, *Nonlinear Optics*, 2nd ed. (Academic, 2003).
12. J. Y. Zhang, C. K. Lee, J. Y. Huang, and C. L. Pan, "Sub femto-joule sensitive single-shot OPA-XFROG and its application in study of white-light supercontinuum generation," Opt. Express **12**, 574–581 (2004).
13. Y. R. Shen, *The Principles of Nonlinear Optics* (Wiley, 1984).
14. A. Smith, "Group-velocity-matched three-wave mixing in birefringent crystals," Opt. Lett. **26**, 719–721 (2001).
15. M. A. Dreger and J. K. McIver, "Second-harmonic generation in a nonlinear, anisotropic medium with diffraction and depletion," J. Opt. Soc. Am. B **7**, 776–784 (1990).
16. N. Bloembergen, *Nonlinear Optics*, 4th ed. (World Scientific, 1996).
17. J.-C. Diels and W. Rudolph, *Ultrashort Laser Pulse Phenomena* (Academic, 1996).
18. A. V. Smith, SNLO Nonlinear Optics Code (Sandia National Laboratories, Albuquerque, N.M. 87185-1423).
19. R. Trebino, "Geometrical issues: single-shot FROG," in *Frequency-Resolved Optical Gating: The Measurement of Ultrashort Laser Pulses*, R. Trebino, ed. (Kluwer Academic, 2002), pp. 141–156.
20. X. Gu, L. Xu, M. Kimmel, E. Zeek, P. O'Shea, A. P. Shreenath, R. Trebino, and R. S. Windeler, "Frequency-resolved optical gating and single-shot spectral measurements reveal fine structure in microstructure-fiber continuum," Opt. Lett. **27**, 1174–1176 (2002).
21. A. L. Gaeta, "Nonlinear propagation and continuum generation in microstructured optical fibers," Opt. Lett. **27**, 924–926 (2002).
22. J. M. Dudley, X. Gu, L. Xu, M. Kimmel, E. Zeek, P. O'Shea, R. Trebino, S. Coen, and R. S. Windeler, "Cross-correlation frequency resolved optical gating analysis of broadband continuum generation in photonic crystal fiber: simulations and experiments," Opt. Express **10**, 1215–1221 (2002).